TOXICOLOGICAL SCIENCES **118(1)**, 236–250 (2010)
doi:10.1093/toxsci/kfq228
Advance Access publication July 28, 2010

The Phototoxicity of Fluvastatin, an HMG-CoA Reductase Inhibitor, Is Mediated by the formation of a Benzocarbazole-Like Photoproduct

Giampietro Viola,*[,1] Pawel Grobelny,† Maria A. Linardi,* Alessia Salvador,‡ Giuseppe Basso,* Jadwiga Mielcarek,§ Stefano Dall'Acqua,‡ Daniela Vedaldi,‡ and Francesco Dall'Acqua‡

*Laboratory of Oncohematology, Department of Pediatrics, University of Padova, 35128 Padova, Italy; †Department of Pharmaceutical Technology, Poznan University of Medical Sciences, 60-780 Poznań, Poland; ‡Department of Pharmaceutical Sciences, University of Padova, 35131 Padova, Italy; and §Department of Inorganic and Analytical Chemistry, Poznan University of Medical Sciences, 60-780 Poznań, Poland

[1]To whom correspondence should be addressed at Laboratory of Oncohematology, Department of Pediatrics, University of Padova, Via Giustiniani 3, 35128 Padova, Italy. Fax: +39-49-8211462. E-mail: giampietro.viola.1@unipd.it.

Received April 28, 2010; accepted July 14, 2010

In this paper, we have investigated the mechanism of phototoxicity of fluvastatin, an 3-hydroxy-3-methylglutaryl coenzyme A reductase inhibitor, in human keratinocytes cell line NCTC-2544. Fluvastatin underwent rapid photodegradation upon Ultraviolet-A (UVA) irradiation in buffered aqueous solution as shown by the changes in absorption spectra. Interestingly, no isosbestic points were observed but only a fast appearance of a spectral change, indicative of the formation of a new chromophore. The isolation and characterization of the main photoproduct revealed the formation of a polycyclic compound with a benzocarbazole-like structure. This product was also evaluated for its phototoxic potential. Cell phototoxicity was evaluated by 3-(4,5-dimethylthiazol-2-yl)-2,5 diphenyl tetrazolium bromide test after 72 h from the irradiation in the presence of fluvastatin. The results showed a reduction of the cell viability in a concentration and UVA dose-dependent manner. Surprisingly, the photoproduct showed a dramatic decrease of the cell viability that occurred at concentrations of an order of magnitude lower than the parent compound. Flow cytometric analysis indicated that fluvastatin and its main photoproduct induced principally necrosis as revealed by the large appearance of propidium iodide-positive cells and confirmed also by the rapid drop in cellular adenosine triphosphate levels. Interestingly, a rapid increase of intracellular calcium followed by an extensive cell lipid membrane peroxidation and a significant oxidation of model proteins were induced by fluvastatin and its photoproduct, suggesting that these compounds exerted their toxic effect mainly in the cellular membranes. On the basis of our results, the phototoxicity of fluvastatin may be mediated by the formation of benzocarbazole-like photoproduct that acts as strong photosensitizer.

Key Words: **fluvastatin; phototoxicity; photoproduct; necrosis; lipid peroxidation; protein oxidation.**

There is a significant number of reports indicating that a variety of drugs can elicit undesired side effects, such as phototoxicity, photoallergy, or photocarcinogenicity (Beijersbergen van Henegouwen, 1997; Elisei *et al.*, 2004; Ferguson, 2002; Stahlmann and Lode, 1999; Viola and Dall'Acqua, 2006).

Absorption of sunlight by drug molecules leads to their excited states. This can proceed further to afford drug-derived reactive intermediates or under aerobic conditions reactive oxygen species (ROS). Any of the above short-lived chemical entities may be able to interact with various cellular components, ultimately producing photodamage (Cosa, 2004; Girotti, 2001; Stadtman and Levine, 2003).

The 3-hydroxy-3-methylglutaryl coenzyme A (HMG-CoA) reductase inhibitors (commonly known as ''statins'') are used in the treatment of hypercholesterolemia and are among the most commercially successful drugs (Alexander *et al.*, 2009; Shaw *et al.*, 2009). They interfere with the synthesis of cholesterol by competitively inhibiting the HMG-CoA reductase, the rate-limiting step in *de novo* cholesterol synthesis. In 1987, with the introduction of lovastatin, the statin drug first became available, and since then, there has been a constant effort to introduce new, improved anti-cholesterol compounds.

Lovastatin, pravastatin, and simvastatin are natural derived inhibitors of HMG-CoA reductase, whereas atorvastatin, fluvastatin, rosuvastatin, pitavastatin, and glenvastatin are fully synthetic compounds.

Among natural statins, lovastatin has been described to cause UVA-induced cellular damage in the human keratinocytes (Quiec *et al.*, 1995), although the compound does not absorb light in the UVA range, and therefore, it cannot act as photosensitizers. The mechanisms by which lovastatin could enhance the cellular photodamage is yet not clearly elucidated. It was speculated that this phenomenon was most likely to be explained by lysosomal membrane destabilization and cholesterol deprivation from plasma membrane. Simvastatin is also known to elicit the chronic actinic dermatitis (Holme *et al.*, 2002). However, its phototoxic

mechanism has been not investigated by *in vitro* laboratory assays up to now.

The entirely synthetic HMG-CoA reductase inhibitors are structurally distinct from the natural derivatives, and they are considered to undergo photochemical decomposition. Hitherto, research has been mainly limited to very few reports (Astarita *et al*., 2007; Cermola *et al*., 2006, 2007; Grobelny *et al*., 2009; Mielcarek *et al*., 2005; Montanaro *et al*., 2009).

Fluvastatin (FLV), shown in Figure 1, is a reversible, competitive, and highly specific inhibitor of HMG-CoA and is widely used in the treatment of hypercholesterolemia. The presence of the double bound in the heptanoic acid chain of the compound results in two stereomeric form, *E*- and *Z*-isomers. The active *trans* form is used in the therapy. The drug is considered to be extremely sensitive to light and must be protected from it during storage. Nevertheless, an exhaustive search of the literature indicates that very little attention has been paid to the photochemical behavior of statins, including FLV. A recent study (Cermola *et al*., 2007) reports the structure elucidation of photoproducts formed after solar and UV exposure of the drug in aqueous media, indicating that photocyclization and photooxygenation are the main reactions involved in the formation of the observed products. Therefore, it would be pertinent at this stage to conduct experiments on the phototoxic potential of fluvastatin. Thus, the aim of this work is to evaluate the phototoxic potential of FLV and its main photoproduct in a cultured NCTC-2544 keratinocytes. In order to gain insight into the mechanism of phototoxicity, we have extended our studies on the photochemical damage on protein model *in vitro*.

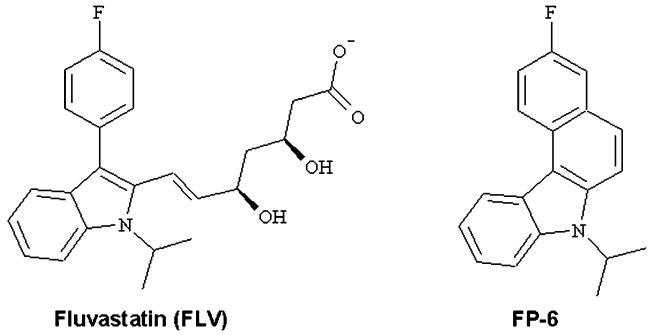

FIG. 1. Structures of FLV and its main photoproducts FP6.

MATERIALS AND METHODS

Chemicals. FLV, [R*,S*-(*E*)]-(±)-7-[3-(4-fluorophenyl)-1-(1-methylethyl)-1H-indol-2-yl]-3,5-dihydroxy-6-heptenoic acid monosodium salt, was obtained from Zydus Cadila (India). Thiobarbituric acid (TBA), sodium azide (NaN_3), N-N′-dimethylthiourea (DMTU), superoxide dismutase (SOD), catalase (CAT), bovine serum albumin (BSA), human serum albumin (HSA), Ribonuclease A (RNAseA), 2,6-di-tert-butylhydroxyanisole (BHA), and glutathione reduced form (GSH) were purchased from Sigma-Aldrich (Milano, Italy).

Irradiation procedure. Two HPW 125 Philips lamps, mainly emitting at 365 nm, were used for irradiation experiments. The spectral irradiance of the source was 4.0 mW/cm^2 as measured at the sample level by a Cole-Parmer Instrument Company radiometer (Niles, IL) equipped with a 365-CX sensor.

***HPLC* analysis and isolation of photoproduct FP-6.** High Performance Liquid Chromatography (HPLC) analyses were carried out on an Agilent 1200 liquid chromatography system (Agilent, Waldron, Germany) consisted of quaternary solvent delivery system, online degasser, autosampler, and a diode array detector. FLV was irradiated in, and its photoproducts were separated at room temperature on a Gemini C18 column (250 × 4.6 mm, 5 μm particle size; Phenomenex, Cheshire, UK). The mobile phase consisted of solvent A (methanol) and solvent B (triethylamine buffer, pH 6.0). Gradient started at 58% vol/vol A held for 5 min ramping up to 65% A over 1 min and then held for 10-min isocratic separation. Subsequently, ramping up to 95% A held for 5 min. The flow rate was 1.0 ml/min and sample injection volume was 5 μl. The chromatographic data were recorded and processed with an Agilent ChemStation workstation. Irradiations of fluvastatin in aqueous buffered solution gave yield of around 25% in terms of FP6 photoproduct. XTerra MS C18 (100 × 19 mm, 5 μm) preparative column was employed for isolation of photoproduct FP6. The mobile phase consisted of solvent A (methanol) and solvent B (water). The gradient elution described above was utilized. Flow rate was 5.0 ml/min, and detection was carried out at 330 nm. The fraction corresponding to FP6 was checked for purity by means of analytical HPLC. Peaks of minor components were detected, but the impurities content never exceeded 2% of the total signal intensity.

Cellular phototoxicity. Phototoxicity experiments were carried out on a immortalized, nontumorigenic cell line of human keratinocytes (NCTC-2544) and a cell line of murine fibroblasts (3T3). Both lines were grown in Dulbecco's Modified Eagle Medium (DMEM) medium (Sigma-Aldrich), supplemented with 115 units/ml of penicillin G, 115 μg/ml streptomycin, and 10% fetal calf serum (Invitrogen, Milan, Italy). The generation time of NCTC-2544 is approximately 21 h. Individual wells of a 96-well tissue culture microtiter plate (Falcon; Becton-Dickinson) were inoculated with 100 μl of complete medium containing 5×10^3 NCTC-2544 or 3T3 cells in exponential growth. The plates were incubated at 37°C in a humidified 5% CO_2 incubator for 18 h prior to the experiments. After medium removal, 100 μl of the drug solution, dissolved in dimethylsulphoxide and diluted with Hank's balanced salt solution (HBSS, pH 7.2), were added to each well and incubated at 37°C for 30 min and then irradiated. After irradiation, the solution was replaced with the medium, and the plates were incubated for 72 h. After this period, control cells reached a confluency of about 90% and the cell viability was assayed by the (3-(4,5-dimethylthiazol-2-yl)-2,5 diphenyl tetrazolium bromide (MTT) test as previously described (Viola *et al*., 2007). Analogous experiments were performed in the presence of different additives.

Cell cycle analysis. For flow cytometric analysis of DNA content, 5×10^5 NCTC-2544 cells in exponential growth were irradiated as described above, and after different times, the cells were trypsinized and together with floating cells, centrifuged, and fixed with ice-cold ethanol (70%). The keratinocytes were then treated with lysis buffer containing RNAseA and subsequently stained with propidium iodide (PI). Samples were analyzed on a Beckman Coulter Cytomic FC500 flow cytometer. For cell cycle analysis, DNA histograms were analyzed using MultiCycle for Windows (Phoenix Flow Systems, CA).

Externalization of phosphatidylserine. Surface exposure of phosphatidylserine (PS) by apoptotic cells was measured by flow cytometry with a Coulter Cytomics FC500 (Beckman Coulter) by adding Annexin-V conjugated with fluorescein isothiocyanate (FITC) to cells according to manufacturer's instructions (Roche Diagnostic, Monza, Italy). Simultaneously, the cells were stained with PI. Excitation was set at 488 nm and the emission filters were set at 525 nm for FITC fluorescence and in the range 560–680 nm for PI fluorescence.

Assessment of mitochondrial changes and production of ROS. The mitochondrial membrane potential was measured with the lipophilic cation 5,5′,6,6′ tetrachlo-1,1′,3,3′-tetraethylbenzimidazol-carbocyanine (JC-1; Molecular Probes

Eugene, OR) (Salvioli *et al*., 1997). Briefly, after different times from the irradiation, the cells were collected by centrifugation and resuspended in HBSS containing the JC-1 at a concentration of 2.5μM. The cells were then incubated at 37°C for 10 min, centrifuged, and resuspended again in HBSS. The fluorescence was directly recorded with the flow cytometer (Coulter Cytomics FC500).

The production of ROS by flow cytometry using hydroethidine (HE) and 2′,7′-dichlorodihydrofluorescein diacetate (H_2DCFDA) (Rothe and Valet, 1990). All these fluorescent probes were purchased from Molecular Probes. After 24 h from the irradiation, the cells were trypsinized and collected by centrifugation and resuspended in HBSS containing the fluorescence probes HE or H_2DCFDA at the concentration of 2.5 and 0.1μM, respectively. As above, the cells were then incubated at 37°C for 30 min, centrifuged, and resuspended again in HBSS. The fluorescence was directly recorded with the flow cytometer using as excitation wavelength 488 nm and emission at 585 nm for HE and at 525 nm for H_2DCFDA.

Detection of DNA fragmentation by agarose gel. Total genomic DNA was extracted from irradiated keratinocytes by a commonly used salting out protocol. One microgram of DNA obtained was subsequently loaded on a 0.8% agarose gel at 50V for 6 h in TAE buffer. After staining in ethidium bromide solution, the gel was washed with water and the DNA bands were detected under UV radiation with a ImageQuant 300 transilluminator (GE Healthcare) equipped with a CCD camera.

ATP assay. Cells were irradiated in the presence of FLV or its photoproduct. After different times from the irradiation, cells were collected and counted and then the ATP content per 100,000 cells was determined using the CellTiter-Glo luminescent assay (Promega, Milano, Italy) according to manufacturer instruction, using a Victor^3 luminometer (Perkin Elmer). Data are normalized to ATP content in nonirradiated cells.

Intracellular calcium measurement. Intracellular calcium in NCTC-2544 cells was measured by flow cytometry using the Ca^{2+}-sensitive fluorescent dye Fluo-4/AM (Molecular Probes). Briefly, irradiated cells after different times were washed and incubated with 2.5μM Fluo-4/AM in complete medium at 37°C for 30 min. The cells were then trypsinized, washed two times, and resuspended in HBSS. The intracellular calcium was analyzed immediately for Fluo-4/AM fluorescence intensity by flow cytometry.

Lysosomal integrity assay. Cells were irradiated in the presence of FLV or the photoproduct, and after different times, the cells were collected by centrifugation and resuspended in DMEM containing the fluorescent probe LysoTracker Red DND-99 (Molecular Probes) at the concentration of 50nM and incubated at 37°C for 30 min. After this period, the cells were washed and analyzed by flow cytometry. As positive control, we incubate the cells with H_2O_2 (Antunes *et al*., 2001) at the concentration of 100μM for 1 h at 37°C and then analyzed as described before.

Detection of the intracellular glutathione content (GSH). Cellular GSH levels were analyzed using 5-chloromethylfluorescein diacetate (CMFDA; Molecular Probes) (Hedley and Chow, 1994). Cell were irradiated in the presence of FLV and incubated for 12 and 24 h, respectively. Cells were harvested, centrifuged, and incubated in the presence of a solution of CMFDA 5μM at 37°C for 30 min. Cytoplasmic esterases convert nonfluorescent CMFDA to fluorescent 6-chloromethylfluorescein which can then react with glutathione. Fluorescence intensity was determined by flow cytometry.

Caspase-3 assay. Caspase-3 activation in NCTC-2544 cells was evaluated by flow cytometry using a human active caspase-3 fragment antibody conjugated with FITC (BD Pharmingen). Briefly after irradiation, the cells were collected by centrifugation and resuspended in Perm/Wash (BD Pharmingen) buffer for 20 min, washed, and then incubated with the antibody for 30 min. After this period, the cells were washed and analyzed by flow cytometry.

Cellular localization studies. NCTC-2544 cells were allowed to attach in a sterile Petri dishes and treated with FLV and FP6 at the concentration of 100 and 50μM, respectively, for 2 h, then washed with HBSS, and incubated for further 30 min in the presence of JC-1, a fluorescence probe that stains mitochondria (Salvioli *et al*., 1997) or LysoTracker Red as fluorescent probe to stain lysosomes (Yuan *et al*., 2002). Cellular fluorescence images were acquired with an video confocal microscope (NIKON), using a Nir Apo 60X/1.0W water immersion objective (NIKON). Emission filter settings were used to separate the emission of the probes from that of the test compounds.

Lipid peroxidation: TBARS assay. Lipid peroxidation was measured using a TBA assay as described previously (Morliére *et al*., 1991). A standard curve of 1,1,3,3-tetraethoxypropane was used to quantify the amount of produced malonaldehyde. Data are expressed in terms of nanomoles of TBARS normalized to the total protein content, measured in an aliquot of the cell extract.

Protein oxidation. Solutions of BSA, RNAseA, and HSA (0.5 mg/ml) in phosphate buffer 10mM were irradiated in the presence of the test compounds for various time in a quartz cuvette. At different time, an aliquot of the solution was taken and the degree of protein oxidation was monitored spectrophotometrically, as described previously (Levine *et al*., 1990), by derivatization with 2,4-dinitrophenylhydrazine (DNPH).

Statistical analysis. Unless indicated differently, the results are presented as mean ± SEM. The differences between irradiated and nonirradiated sample were analyzed, using the two-sided Student's *t*-test.

RESULTS

Isolation and Characterization of the Photoproducts

FLV showed absorption maxima in the UVA range (320–400 nm) and underwent rapid photodegradation upon UVA irradiation in buffered aqueous solution as previously reported (Cermola *et al*., 2007; Mielcarek *et al*., 2005). No distinct isosbestic points were observed, but just after low UVA doses (0.5–2.5 J/cm^2), the appearance of a spectral change was detected, indicative of the formation of a new chromophore or multiple products (Supplementary data).

More importantly, a detailed kinetic analysis, carried out by HPLC (Fig. 2), showed that FLV was completely degradated yielding multiple products, after 7.5 J/cm^2 of UVA, corresponding to 30 min of irradiation in our conditions. The UV spectra of FP1–FP2 and FP3–FP4 presented in Figure 2 were indistinguishable with λ_{max} 260 and 280 nm, respectively, suggesting that the pair of the photoproducts possessed similar structure of chromophore. In addition, the UV spectrum of FP6 was very similar to that of FP3, except for a slight red shift of λ_{max} and much more different polarity. We assumed similar structure of the chromophores differing only in an additional side chain responsible for polarity. However, the majority of them appear to be unstable. Fractions corresponding to six photoproduct (FP1–FP6) were isolated. The dried fractions were dissolved in methanol and analyzed by mass spectrometry. The mass spectra were recorded over the range 100–1000 *m/z* in the positive mode (Supplementary data).

We focused our attention on the isolation and characterization of product FP6 because this compound was formed in high quantity and after prolonged irradiation was the only product found (Cermola *et al*., 2007). Isolated fraction corresponding to FP6 was dissolved in methanol (MeOH-d_4) and subjected to

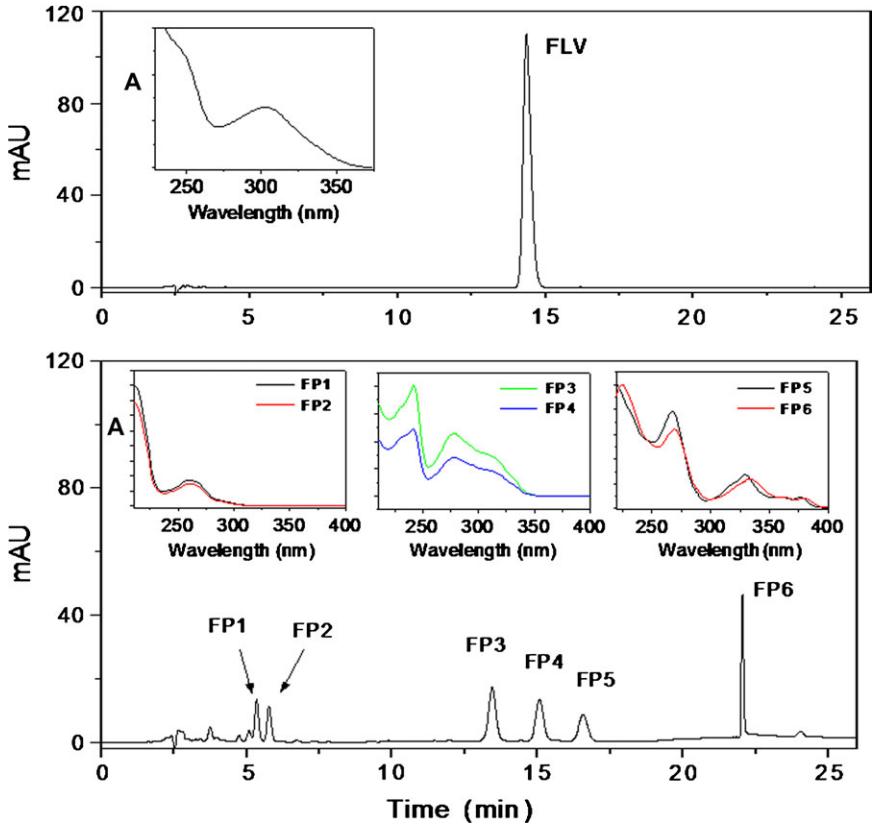

FIG. 2. Representative HPLC chromatograms obtained from aqueous solution of FLV exposed to 0 (panel A) or 7.5 J/cm^2 of UVA (panel B). The inset in the chromatogram represents absorption spectra of FLV (panel A) and its photoproducts FP1–FP6 (panel B).

^{1}H-NMR and Correlation Spectroscopy (^{1}H,^{1}H COSY-NMR) analyses. NMR spectra (see Supplementary data) indicated a structure consistent with a tetracyclic compound namely 9-fluoro-5-(1-methylethyl)-benzo[*c*]carbazole depicted in Figure 1. These findings are in excellent agreement with the paper of Cermola *et al*. (2007), who reported the isolation and a detailed characterization of fluvastatin photoproducts after solar and UVA irradiation in aqueous solution.

Cellular Phototoxicity

The phototoxicity of FLV was evaluated in a cell line of immortalized human keratinocytes NCTC-2544 by use of the MTT assay carried out 72 h after irradiation. Figure 3 (panel A) shows the reduction of viability obtained in NCTC-2544 cells at different concentration and different UVA doses. As can be observed, a concentration and UVA dose-dependent reduction of cell viability is induced by FLV. The calculated GI_{50} were > 100, 99.1 18.5, and 5.5μM at the UVA doses of 1.25, 2.50, 3.75 and 7.5 J/cm^2, respectively. In the same experimental conditions but in the absence of irradiation, FLV did not show any decrease of viability.

In the same model, photoproduct FP6 was tested. FP6 did not affect cell viability without irradiation but on the contrary, after irradiation a dramatic reduction of cell viability can be observed for this compound in comparison to the parent one, as showed in Figure 3 (panel B). In this case, the calculated GI_{50} were 3.7, 1.9 and 1.3μM at the UVA doses of 1.25, 2.50, and 3.75 J/cm^2, respectively.

Analogous experiments were performed also in 3T3 fibroblast cell line, a well-known *in vitro* model to evaluate the phototoxic potential of a drug (Spielmann *et al*., 1998).

Also in this cell line we have observed a clear reduction of cell viability that is both UVA dose and concentration dependent. In comparison to human keratinocytes, 3T3 appear more sensible to the phototoxic action of FLV because the GI_{50} in this cell line are lower than that observed in NCTC-2544 cells (82.8, 31, and 8.5μM at at the UVA doses of 1.25, 2.50, and 3.75 J/cm^2, respectively). On the contrary, the sensitivity of 3T3 to FP6 appear similar to NCTC-2544 cells, in fact the GI_{50} are in this case 11.5, 6.8 and 3.1μM at the UVA doses of 1.25, 2.50, and 3.75 J/cm^2, respectively, although also in this case a remarkable increase of phototoxicity was observed in comparison to the lead compound. Altogether these data suggest that the phototoxicity of FLV could be mediated by the formation of this photoproduct.

With the purpose to evaluate which reactive species are involved in the mechanisms of photoinduced cell toxicity, analogous experiments were performed, irradiating NCTC-2544

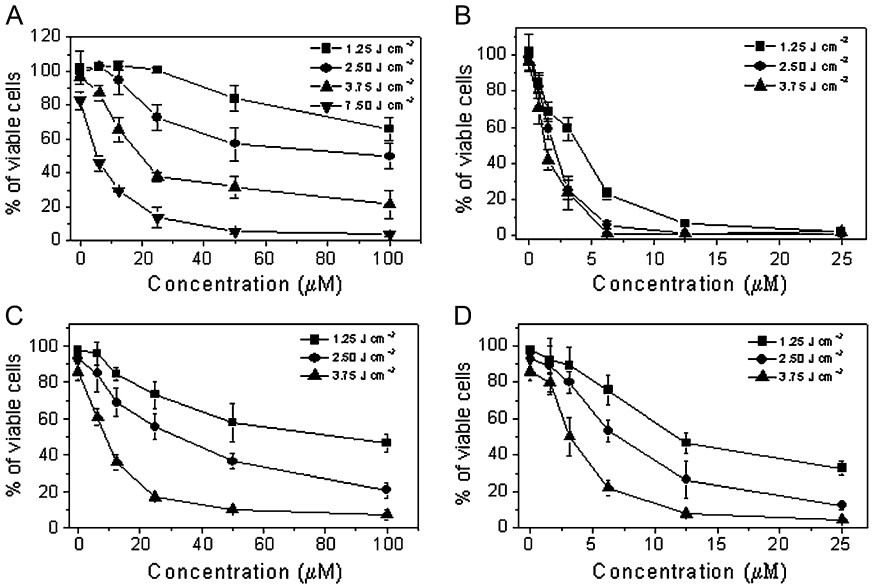

FIG. 3. Percentage of viability of NCTC-2544 human keratinocytes (panels A and B) and 3T3 murine fibroblast (panels C and D) after UVA irradiation in the presence of FLV (panels A and C) and photoproduct FP6 (panels B and D). Cells were irradiated at the indicated different UVA doses and at different concentrations of drugs. Cell viability was measured by MTT test after 72 h after irradiation. Data represent mean ± SEM for at least four independent experiments.

cells with FLV and FP6 in the presence of different scavengers as previously reported (Elisei *et al*., 2004; Viola *et al*., 2007). The additives used were NaN_3 (a singulet oxygen scavenger), SOD (scavenger of $O^{\bullet -}$), CAT (scavenger of H_2O_2), mannitol and DMTU (scavengers of $^{\bullet}OH$), and BHA and GSH (free radical scavengers). The concentrations of the compounds and the UVA doses were chosen on the basis of the results presented in Figure 3.

It can be observed from Table 1 that the photoinduced cell death by FLV and FP6 is efficiently counteract by SOD, GSH, BHA, and mannitol, indicating that superoxide anion and free and hydroxyl radicals may be involved in the mechanism of action.

Assessment of the Mode of Cell Death

To characterize the mode of cell death (necrosis or apoptosis) photoinduced by FLV and its photoproduct FP6, a biparametric cytofluorimetric analysis was performed to quantify the precise extent of apoptosis versus necrosis using PI, which stains DNA and is permeable only to dead cells, and fluorescent immunolabeling of the protein Annexin-V, which binds to PS in a highly selective manner. This phospholipid flips from the inner to the outer leaflet of the plasma membrane during apoptosis. Positive staining with Annexin-V correlates with the loss of plasma membrane polarity but precedes the complete loss of membrane integrity that accompanies the later stages of cell death resulting from either apoptosis or necrosis. In contrast, PI can only enter cells after the loss of their membrane integrity. Thus, dual staining with Annexin-V and PI allows clearly to discriminate between unaffected cells (Annexin-V^-/PI^-), early apoptotic cells (Annexin-V^+/PI^-), late apoptotic cells (Annexin-V^+/PI^+), and necrotic cells (Annexin-V^-/PI^+)(Vermes *et al*., 1995).

Figure 4 (panel A) shows, as representative, four biparametric histograms in which the effect of FLV at 6 and 24 h from the irradiation is depicted. It is quite evident that FLV early induced an accumulation of PI-positive cells in

TABLE 1
Effects of different scavengers on the phototoxicity induced in NCTC-2544 cells, by fluvastatin and FP6

Treatment (concentration, UVA dose)	Scavenger (concentration)	% Cell viability
FLV (25μM, 3.75 J/cm^2)	None	36.8 ± 4.5
	BHA (10μM)	37.4 ± 4.6
	NaN_3 (20mM)	33.0 ± 4.0
	DMTU (1mM)	39.9 ± 4.9
	GSH (1mM)	66.6 ± 7.1**
	CAT (1000 UI/ml)	37.1 ± 4.4
	SOD (2000 UI/ml)	59.1 ± 8.4*
	Man (10mM)	88.9 ± 8.7**
FP6 (5μM, 1.25 J/cm^2)	None	65.6 ± 5.2
	BHA (10μM)	89.4 ± 6.4*
	NaN_3 (20mM)	62.6 ± 5.4
	DMTU (1mM)	88.2 ± 4.6*
	GSH (1mM)	96.3 ± 7.5**
	CAT (1000 UI/ml)	67.6 ± 3.9
	SOD (2000 UI/ml)	77.1 ± 4.6*
	Man (10mM)	87.3 ± 6.2*

Note. The cell viability was measured 72 h from the treatment with the MTT test.

*$p < 0.05$; **$p < 0.01$ versus none Student's *t*-test ($n = 5$).

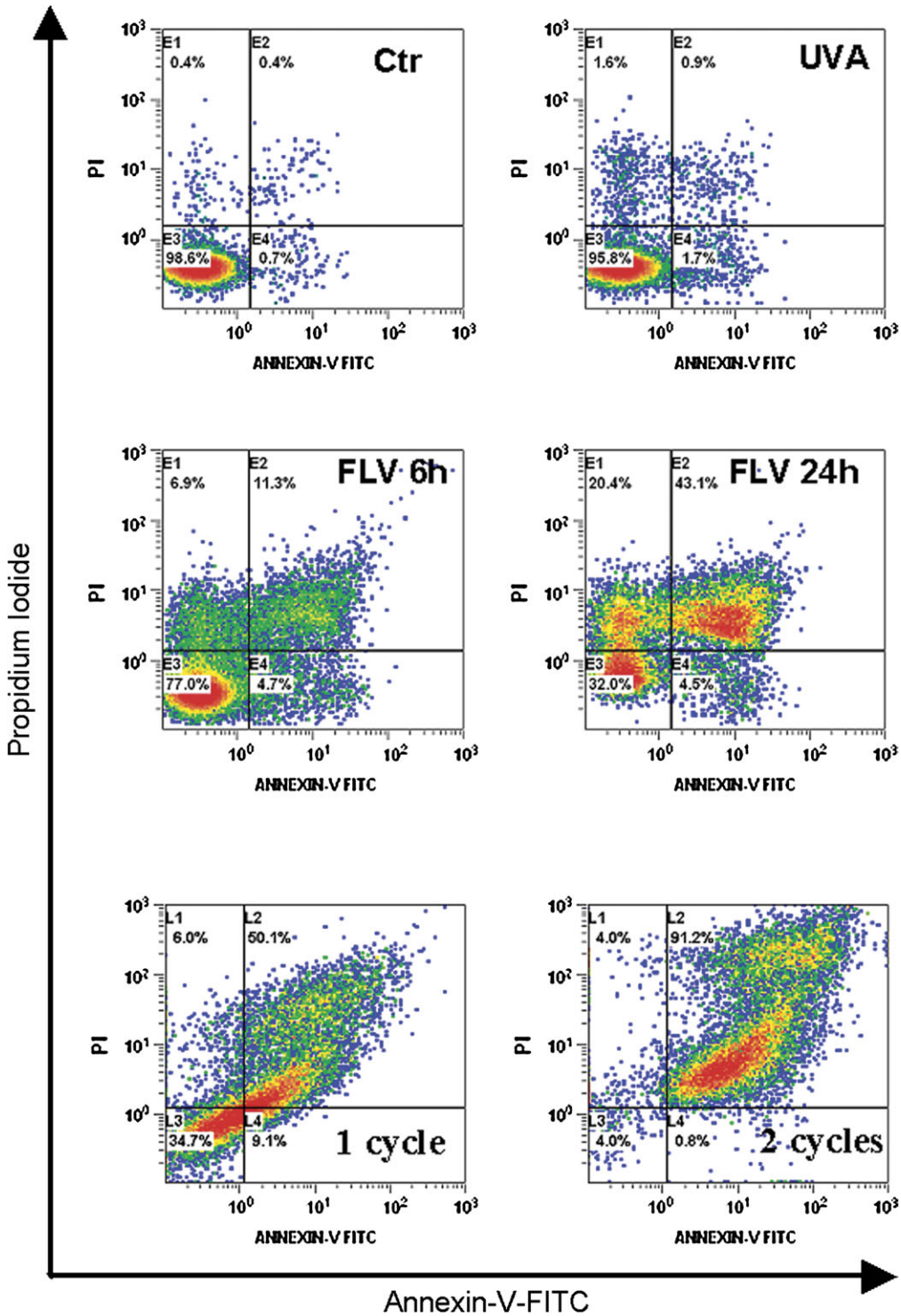

FIG. 4. Determination of the mode of cell death using Annexin-V and PI staining and flow cytometric analysis. (Panel A) Representative biparametric histograms obtained after 6 and 24 h after the irradiation (3.75 J/cm^2) of NCTC-2544 cells in the presence of FLV 50μM. (Panels B and C) Representative histograms of necrotic NCTC-2544 cells generated by one (panel B) or two cycles (panel C) of a rapid freeze/thaw exposure of the cells.

comparison to the irradiated control and these latter further increase at 24 h, indicating the formation of necrotic cells. As positive control, we submitted the cells to rapid cycles of freeze/thawing, and the histograms depicted in Figure 4 (panels B and C) show that the cell population after this treatment was composed exclusively of necrotic cells (i.e., Annexin-V$^+$/PI$^+$).

A complete picture of results is presented in Figure 5 for FLV at the concentration of 50 and 25μM and in Figure 6 for FP6 at the concentration of 10 and 5μM. It can be observed that we did not observed A^+/PI^- cells at any time point investigated, but, on the contrary, a large percentage of PI-positive cells was found indicating a rapid permeabilization of the cell plasma membrane that leads to a necrotic cell death.

The mode of cell death was also followed by two most common end point analysis such as morphological changes and analysis of DNA fragmentation (Galluzzi *et al*., 2009). As shown in Figure 7 (panel A), visual inspection by contrast phase microscopy of the morphology of NCTC-2544 cells irradiated in the presence of FLV (50μM) or FP6 (10μM) revealed the presence of cellular swelling and rupture of the plasma membrane which are typical signs of necrotic type of cell death. Furthermore, agarose gel electrophoresis of DNA extracted from keratinocytes irradiated in the presence of FLV and FP6 (Fig. 7, panel B) showed a nonspecific degradation resulting in a ''smear'' of randomly degraded DNA in the samples treated, indicative of a necrotic cell death. In addition, we evaluated the activity of caspase-3 because this enzyme is essential to the propagation of the apoptotic signal after the exposure to many DNA-damaging agents and anticancer drugs, and it is activated in most cases of photodynamic therapy with a number of different photosensitizers (Kumar, 2007; Oleinick *et al*., 2002; Porter and Janicke, 1999). As depicted in figure 7 (panel C), flow cytometric analysis of NCTC-2544 irradiated in the presence of FLV and FP6 did not show any activation of caspase-3.

ATP Assay

Apoptosis is an energy-dependent process in which the decrease of ATP below critical levels may impede the execution of apoptosis and promote necrosis (Eguchi *et al*., 1997; Leist *et al*., 1997). In fact, necrosis is characterized by a rapid drop in ATP and given the potentially pivotal role attributed to ATP in the necrosis, we measured cellular ATP levels following irradiation with FLV and FP6.

Using a luciferase-based assay for cellular ATP content, a dramatic depletion of ATP levels was detected in keratinocytes-irradiated cells in the presence of 50μM FLV (Fig. 8). Similarly, the irradiation with 10μM FP6 dramatically decreases ATP levels in comparison to nonirradiated cells: this was already seen after 6 h from irradiation, and a further reduction was detected at 24 h reaching levels of around 10%. Taken together, these data suggested that the rapid and pronounced ATP depletion was a concurrent event that accompanied the loss of cell viability.

Analysis of Cell Cycle

To investigate the effects of FLV and FP6 upon UVA irradiation on the cell cycle, NCTC-2544 cells were treated with the test compounds at different concentrations and at the light dose of 3.75 J/cm^2. After 12, 24, and 48 h from the

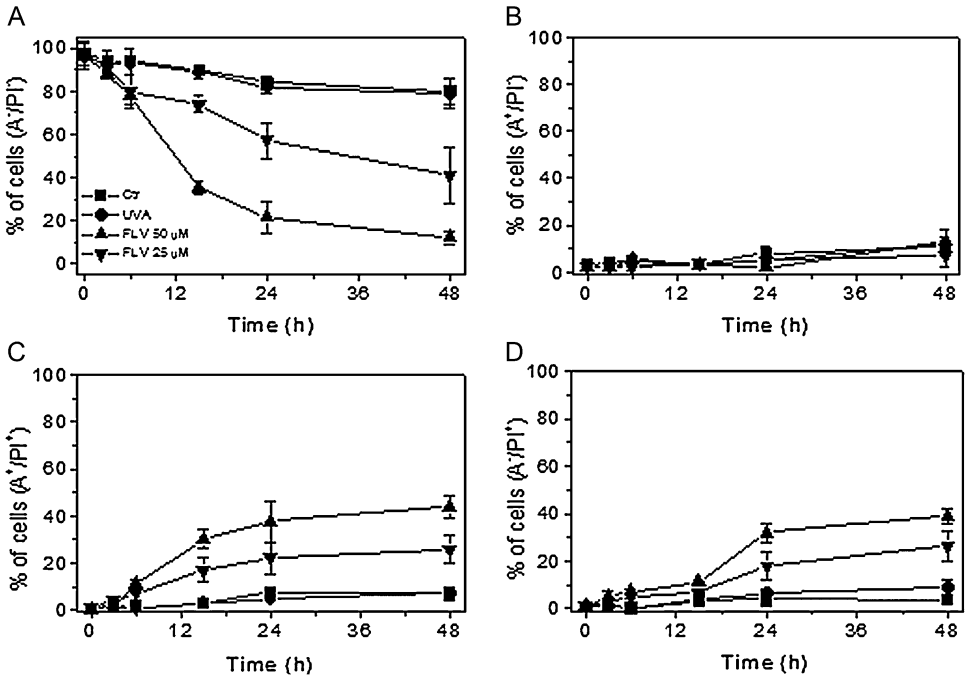

FIG. 5. NCTC-2544 cells were irradiated in the presence of FLV at the indicated concentration, and after different times, the cells were collected and stained with Annexin-V-FITC and PI and analyzed by flow cytometry. The results are expressed as percentage of cells found in the different region of the biparametric histograms showed in figure 4. Panel A: A^-/PI^- cells; panel B: A^+/PI^-; panel C: A^+/PI^+; panel D: A^-/PI^+. Data represent mean ± SEM of three independent experiments.

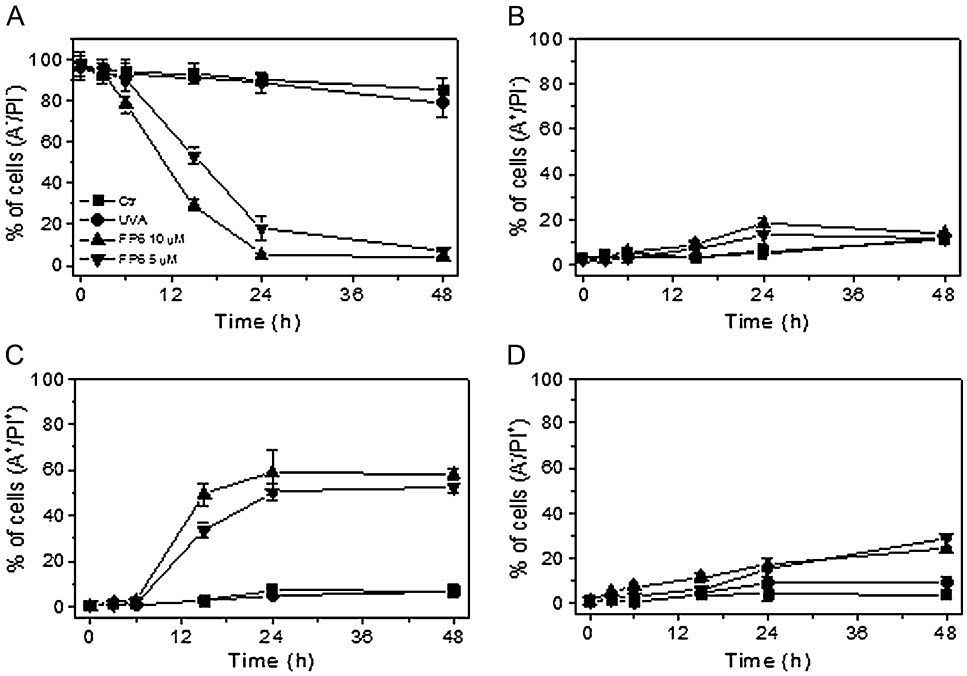

FIG. 6. NCTC-2544 cells were irradiated in the presence of FP6 at the indicated concentration, and after different times, the cells were collected and stained with Annexin-V-FITC and PI and analyzed by flow cytometry. The results are expressed as percentage of cells found in the different region of the biparametric histograms showed in figure 4. Panel A: A^-/PI^- cells; panel B: A^+/PI^-; panel C: A^+/PI^+; panel D A^-/PI^+. Data represent mean ± SEM of three independent experiments.

irradiation, the cells were fixed and labeled with PI. The different phases of the cell cycle were analyzed by flow cytometry.

Irradiation of keratinocytes with the FLV and its photoproduct induced only a modest increase of the S phase along with a reduction of G1 phase (Table 2) in particular at 24 h. More importantly, it is interesting to note that the percentage of the cell population with hypodiploid DNA content peak (sub-G1) reached a maximum value of 10–20% at 24 h. This peak represents those cells with a DNA content less than G1, usually considered as apoptotic cells slightly increased in the treated samples in comparison to the controls.

Mitochondrial and Lysosomal Integrity Assessment

To investigate which cellular sites are involved in the phototoxicity induced by FLV and FP6, we focused our attention on mitochondria and lysosomes. It has been previously shown that mitochondrial and/or lysosomal alterations are involved in cell death caused by many photosensitizers including fluoroquinolones, phenothiazines, antimalarial drugs, and porphyrins (Kessel and Luo, 2001; Ouedraogo *et al*., 1999; Viola and Dall'Acqua, 2006; Viola *et al*., 2007). In an attempt to evaluate the intracellular localization of FLV and its photoproduct in NCTC-2544 cells, we used two fluorescent probes: JC-1, a lipophilic cation commonly used for the assessment of the mitochondrial potential (Salvioli *et al*., 1997), and LysoTracker RED, a fluorescent dye that specifically stains lysosomes (Yuan *et al*., 2002), while the test compounds emit in the blue region. Both fluorescences can be easily separated using suitable bandpass optical filters. It can be observed in Figure 9 that both FLV and FP6 were found to incorporate into NCTC-2544 cells and distribute within the cytoplasm after incubation but without a specific disposition into subcellular structures as evidenced by the loss of overlapping with JC-1 and LysoTracker Red.

Further experiments to assess changes in mitochondrial functions after irradiation in the presence of FLV and FP6 were performed measuring mitochondrial potential ($\Delta\psi_{mt}$), by flow cytometry, using the JC-1 dye which is considered a reliable probe to assess such events (Salvioli *et al*., 1997). Flow cytometric analysis of NCTC-2544 cells after 12, 24, or 48 h from the irradiation in the presence of the compounds showed no significant variations (Supplementary data) of $\Delta\psi_{mt}$ in comparison to the irradiated control, indicating the non-involvement of this organelle in the photoinduced cell death. To confirm that mitochondria were not involved in the photokilling mechanism, we also evaluated the mitochondrial production of ROS by two fluorescent probes, HE and H_2DCFDA by flow cytometry (Nohl *et al*., 2005; Rothe and Valet, 1990). In agreement, only a slight increase of ROS production was observed for cell irradiated with FLV and FP6 (Supplementary data).

In order to investigate the integrity of lysosomes after irradiation with the test compounds, flow cytometric analysis was performed using the fluorescent acidotropic dye LysoTracker Red.

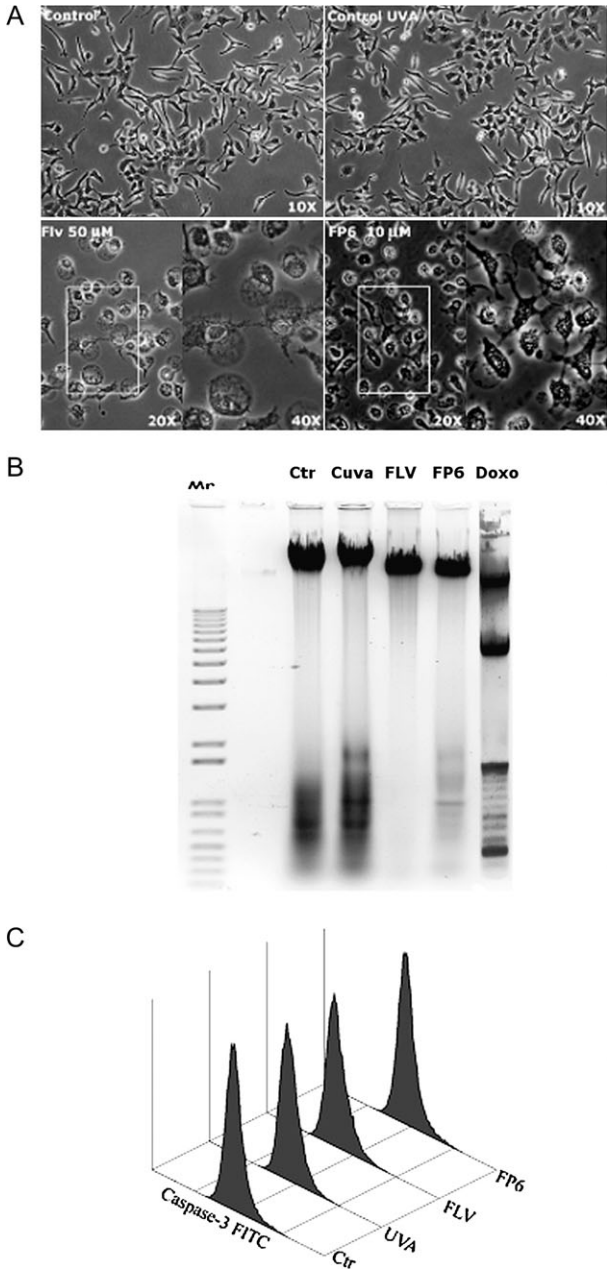

FIG. 7. Panel A) Cell micrographs taken after 24 h from the irradiation (3.75 J/cm^2) in the presence of FLV and FP6 at the indicated concentrations. (Panel B) Agarose gel electrophoresis of chromosomal DNA extracted from NCTC-2544 cells 24 h after the irradiation (3.75 J/cm^2) in the presence of FLV (50µM) and FP6 (10µM) or after 24 h of treatment with doxorubicin 5µM. Lane 1: control (Ctr); lane 2: UVA; lane 3: FLV (50µM); lane 4: FP6 (10µM); and lane M indicated size marker DNAs. (Panel C) Flow cytometric analysis of caspase-3 activity after irradiation in the presence of FLV (50µM) and FP6 (10µM). After 24 h of treatment, cells were harvested and stained with an anti-human active caspase-3 fragment monoclonal antibody conjugated with FITC. Representative histograms of three different experiments are shown.

As showed in Figure 10 (panels A and B), the irradiation of the cells in the presence of FLV led to a reduction of LysoTracker fluorescence that occurred just after 6 h from it, indicating

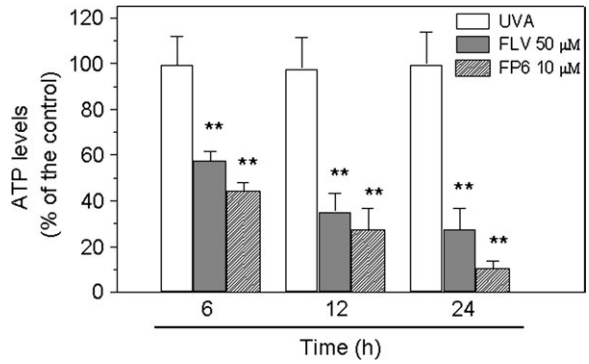

FIG. 8. ATP levels were measured in NCTC-2544 cells after different times from the irradiation (3.75 J/cm^2) in the presence of FLV (50µM) and FP6 (10µM). Data represent mean ± SEM of three independent experiments. $^{**}p <$ 0.01 versus UVA-irradiated cells.

alterations of the lysosomal membrane permeability. Interestingly, this effect did not occur with FP6, if not at later time in comparison to FLV probably because of a different disposition of the photoproduct.

Intracellular Ca^{2+} Measurement

It has been demonstrated that the overload of intracellular Ca^{2+} is associated with necrotic cell pathway (Golstein and Kroemer, 2007). To verify whether a calcium signal is involved in the photoinduced cell death mechanism activated by FLV and FP6, we used the Ca^{2+}-sensitive dye Fluo-4/AM to investigate whether FLV and FP6 induce an increase in intracellular Ca^{2+} concentration in NCTC-2544 cells. The cells displayed an increase in Fluo-4/AM fluorescence intensity just after 1 h from irradiation, and the intensity was two to three times greater that the irradiated controls for both FLV and its photoproduct (Fig. 11).

To verify the source of calcium, we performed similar experiment using a calcium-free medium containing 1mM ethylene glycol tetraacetic acid (EGTA). The results showed (Fig. 11, panel C) that in these experimental conditions a significant decrease of fluorescence occurred, indicating that the increased intracellular calcium is because of calcium influx from the extracellular sites without calcium release from internal stores.

Lipid Peroxidation and GSH Content Assay

To gain insight into the photoinduced cell death mechanism activated by FLV and FP6, we investigated if these compounds cause lipid peroxidation by measuring the level of malonyldialdehde (MDA) bound to TBA in treated and untreated NCTC-2544. This assay is a measure of membrane injury as the cellular level of MDA correlates with lipid peroxidation. The results showed (Fig. 12, panel A) that in untreated cells or in UVA-irradiated cells, the levels of TBARS were relatively low, in contrast the levels of TBARS increased significantly just after 6 h after the irradiation in the presence of FLV and

TABLE 2
Effect of FLV and FP6 on the cell cycle of NCTC-2544

	% G1[a]	G2/M	S	Apoptotic cells[b] (sub-G1)
Ctr, 12 h	65.1 ± 2.0	11.0 ± 1.9	25.6 ± 1.7	1.8 ± 0.1
UVA alone, 12 h	64.6 ± 3.0	10.0 ± 1.5	25.4 ± 2.1	1.3 ± 0.3
FLV, 12 h, 50μM	61.0 ± 4.0	7.7 ± 2.5	31.3 ± 4.1	6.9 ± 1.5
FP6, 12 h, 10μM	58.9 ± 5.2	19.8 ± 1.5	32.3 ± 3.5	2.5 ± 0.7
Ctr, 24 h	63.2 ± 3.4	11.6 ± 1.2	25.2 ± 2.8	1.0 ± 0.3
UVA alone, 24 h	66.9 ± 3.5	14.1 ± 3.1	19.0 ± 1.5	5.4 ± 1.9
FLV, 24 h, 50μM	43.9 ± 2.7	15.6 ± 1.0	40.4 ± 3.0	12.1 ± 4.3
FP6, 24 h, 10μM	60.4 ± 11.1	10.1 ± 5.8	29.5 ± 5.7	20. 9 ± 5.5
Ctr, 48 h	62.8 ± 1.2	10.4 ± 2.9	26.8 ± 1.6	5.0 ± 1.5
UVA alone, 48 h	63.4 ± 2.7	9.8 ± 0.5	26.6 ± 2.3	5.2 ± 1.0
FLV, 48 h, 50μM	52.5 ± 5.6	17.8 ± 2.1	29.7 ± 3.5	6.6 ± 2.1
FP6, 48 h, 10μM	50.5 ± 2.5	19.5 ± 1.5	30.9 ± 6.2	10.5 ± 3.1

Note. Ctr, control.
[a]The percentage of each phase of the cell cycle was calculated on living cells.
[b]Percentage of the cell population with hypodiploid DNA content peak (apoptotic cells).

then further augmented at later times. On the contrary, the effect of FP6 on lipid peroxidation became significant after 12 h from irradiation although less marked in comparison to the parent compound. Therefore, lipid peroxidation initiated by photoactivated FLV is well correlated with the increase of cell permeability to PI.

The photoinduced lipid peroxidation also occurred in a concentration-dependent way as depicted in Figure 12 (panel B) after 24 h from the irradiation the levels of TBARS increased of about 10 times for FLV at the concentration of 50μM and decrease proportionally with 25 and 12.5μM. In the case of FP6, the increase of TBARS was about three times at the concentration of 10μM and decreased at the concentration of 5μM. Thus, the induced oxidative damage to membrane lipids is well correlated with the extent of cell death, suggesting that an extensive lipid peroxidation could play a major role in the photokilling mechanism.

We investigated whether the induction of lipid peroxidation may be linked to a reduction of intracellular glutathione (GSH) levels. GSH plays a central role in the defence of cells against ROS and is a potent factor in the control of lipid peroxidation (Higuchi, 2004; Kim *et al*., 2005). Indeed, the depletion of GSH after irradiation became significant both for FLV and FP6 after 12 h from the irradiation (Fig. 12 panel C), suggesting that a time lag exist between the photoinduction of membrane alteration, which is a rapid process, and the reduction of GSH levels. To confirm that the decrease of GSH may be the consequence of an oxidative stress and not to conjugation reaction with the drugs, we irradiated in aqueous buffered solution of FLV or FP6 and GSH at different molar ratio and the mixture analyzed by LC-MS/MS. The result (data not shown) has showed that the drugs are not able to form conjugates with GSH.

Protein Photodamage

To investigate more deeply the phosensitizing properties of FLV and FP6 toward other components of cellular membranes, such as proteins, aqueous buffered solutions of FLV and FP6 containing BSA, HSA, or RNAse, as models, were irradiated for various times. The degree of oxidative modifications was measured by monitoring the carbonyl content, an index of oxidative damage of the proteins (Levine *et al*., 1990). The results, reported in Figure 13, demonstrated that both FLV and FP6 significantly increased the carbonyl content of BSA and HSA after irradiation.

Irradiated BSA with FLV showed an increase in carbonyl content that is both concentration and UVA dose dependent. A similar picture was observed using HSA as a model protein.

RNAse was selected as a protein model because of the lack of Trp residues together with the presence of Tyr and Phe residues in its sequence. FP6 at the concentration of 10μM did not significantly induce a high degree of protein oxidation using RNAse, reaching at the highest UVA dose used (11 J/cm^2), an increase of the carbonyl content of about 10%. On the contrary, a remarkable increase of protein oxidation was observed with both HSA and BSA.

DISCUSSION

In this work, we have examined the phototoxic effect of fluvastatin, a highly specific inhibitor of HMG-CoA reductase. At the best of our knowledge, this is the first report in which the phototoxic effect of fluvastatin is demonstrated at cellular level. Previous reports (Cermola *et al*., 2007; Mielcarek *et al*., 2005) have investigated the photostability of this drug and the characterization of its photoproducts after UV and solar irradiation. On the basis of these results, we evaluated the phototoxicity in a human cell line of keratinocytes. In our condition, the drug is completely degraded after a UVA dose of 7.5 J/cm^2, and in agreement with Cermola *et al*. (2007), we were able to detect different photoproducts after HPLC analysis. We focused our attention on the isolation of a product of photocyclization (FP6) with the purpose to evaluate its phototoxicity because it is well known that photochemical transformation of drugs leads to different photoproducts that in some cases are more toxic than the parent compound (Beijersbergen van Henegouwen, 1997; Cosa, 2004).

FLV in combination with UVA light induced a reduction of the cell viability, but more importantly, its photoproduct FP6 showed a remarkable increase of the phototoxicity at concentration 10 times lower than the parent compound. It is interesting to note that the UVA doses used for the evaluation of phototoxicity are within the range of UVA doses sufficient to induce the photodegradation of the drug and its photocyclization. Thus, these results strongly suggest that the phototoxicity of FLV could be mediated by the formation of

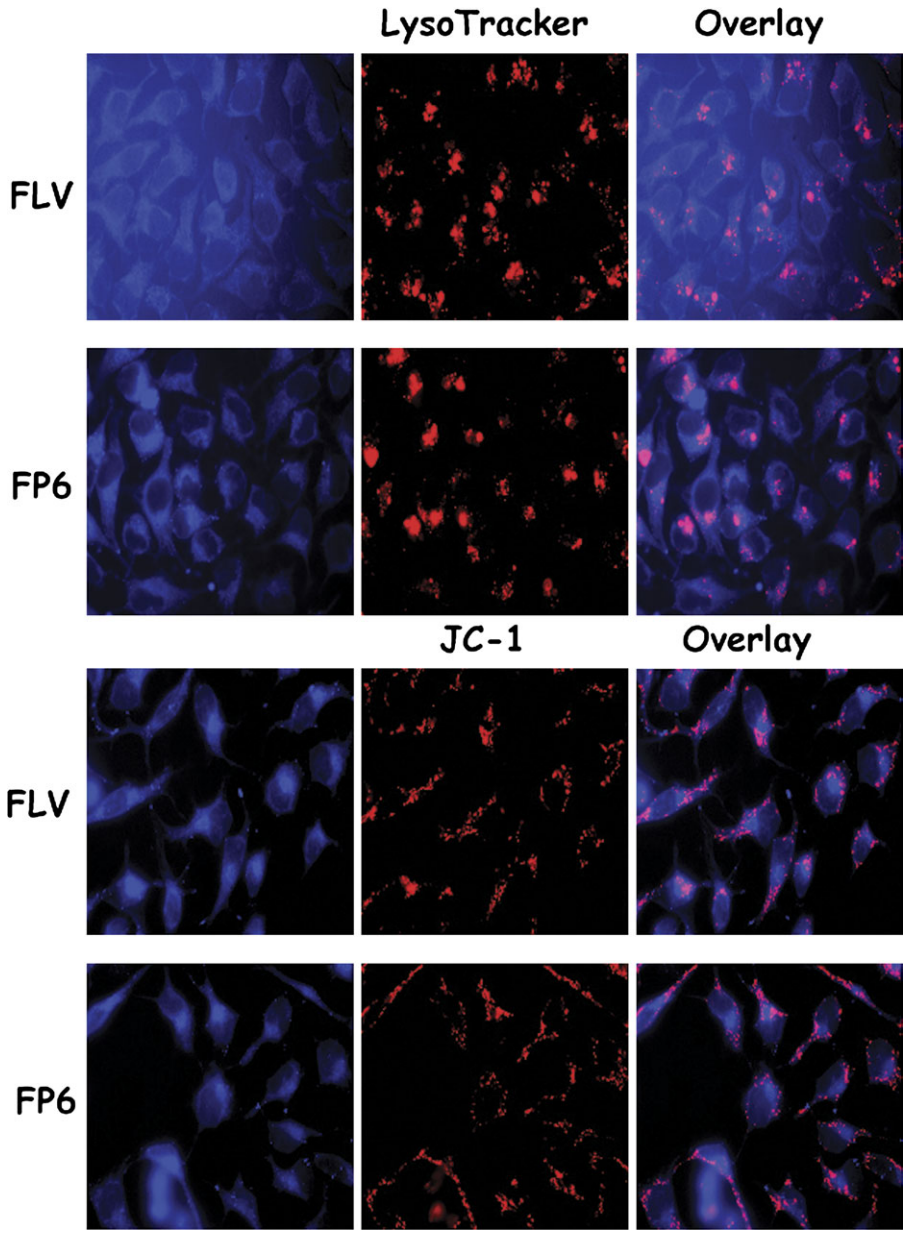

FIG. 9. Intracellular localization of FLV and FP6. (Panel A) Fluorescence microphotographs showing the intracellular localization of FLV and FP6 in NCTC-2544 cells in the presence of JC-1. (Panel B) Fluorescence microphotographs showing the intracellular localization of FLV and FP6 in NCTC-2544 cells in the presence of LysoTracker Red.

a benzocarbazole-like structure (FP6) that acts as a strong photosensitizers.

In our study, the treatment of keratinocytes with BHA, mannitol, and GSH significantly protects from the photoinduced cell death, indicating the involvement of free radicals in the mechanism of action of both FLV and its photoproducts. Interestingly, the addition of an antioxidant enzyme such as SOD protects the cells against the loss of viability, suggesting that $O^{\bullet -}$ is also involved.

Soon after irradiation with FLV, cells initiated a series of profound morphological alterations that affect subcellular organelles and the integrity of the plasma membrane. In contrast, the nuclear structure is preserved, and no DNA degradation is detected. These features are typical necrotic cell death. Necrosis is associated with cell swelling, membrane rupture, and release of cytosolic content to the external environment, whereby the loss of membrane integrity is considered an early event in the process.

To monitor the membrane integrity after irradiation with FLV, we used flow cytometry and double staining with Annexin-V and PI. Annexin-V staining precedes the loss of membrane integrity that accompanies the latest stages of cell

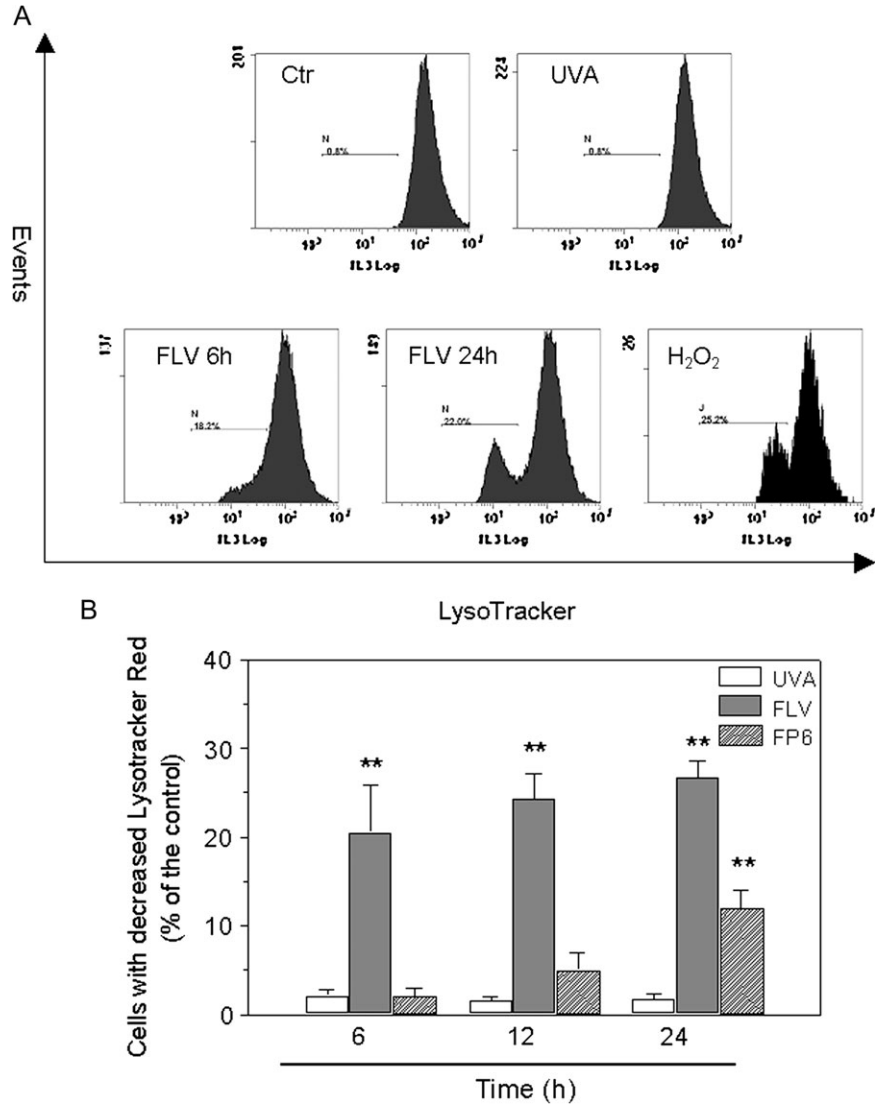

FIG. 10. NCTC-2544 cells were irradiated in the presence of FLV or FP6 and after the indicated times stained with LysoTracker Red and analyzed by flow cytometry. Representative histograms from three independent experiments are shown (panel A); the marker indicates the percentage of cells with damaged lysosomes. As positive control, cell treated with H_2O_2 at the concentration of 100mM for 1 h were also showed. (Panel B) Percentage of cell with reduced LysoTracker fluorescence. Data are expressed as mean ± SEM of three independent experiments $^{**}p < 0.01$ versus UVA-irradiated cells.

death resulting from either apoptotic or necrotic processes. Considering that externalization of PS occurs in the earlier stages of apoptosis, Annexin-V staining identifies apoptosis at an earlier stage than sub-G1 appearance, which represents a later stage of apoptosis being based on nuclear changes such as DNA fragmentation. On the contrary, PI is a plasma membrane impermeant dye. It should be noted that if plasma membrane is permeabilized, Annexin-V can bind to intracellular PS as well (Galluzzi *et al.*, 2009).

Our results showed a rapid increase in the PI-positive cells, whereas Annexin-V–positive cells did not increase significantly at any time investigated. In excellent agreement with the MTT test, the photoproduct FP6 induced high amount of PI-positive cells but at lower concentration respect the parent compound indicating its involvement in the photoinduced cell death.

In this context, we observed a significant increase of intracellular Ca^{2+} concentration soon after the irradiation. Moreover, by depleting extracellular calcium with EGTA, we did not observe an increase of intracellular calcium after irradiation with FLV and FP6, suggesting that the increased intracellular Ca^{2+} was from extracellular sites probably because of a rapid loss of membrane integrity.

The subcellular localization of FLV is not well defined. The FLV molecules were readily detected into cell membranes, and the partition coefficient is consistent with a hydrophobic character. However, FLV is also water soluble and would be expected to also reside in the cytoplasm. Accordingly, we have

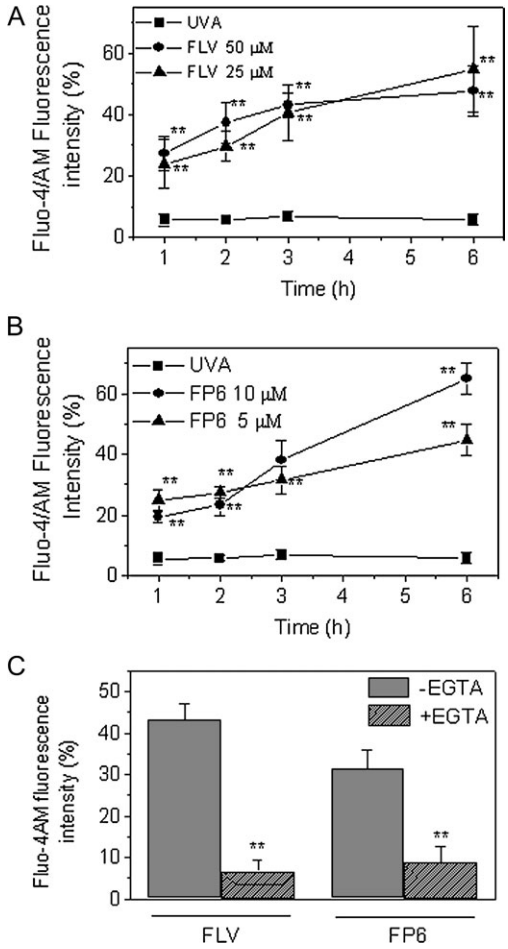

FIG. 11. Intracellular calcium measurement in NCTC-2544 cells after different times from the irradiation (3.75 J/cm^2) in the presence of FLV 50 and 25μM (panel A) and FP6 10 and 5μM (panel B). Ca^{2+} was measured by labeling the cells with 2.5μM of Fluo-4/AM and examining the fluorescence by flow cytometry. Analogous experiments were performed in a calcium-free medium containing 1mM EGTA (panel C) and analyzed after 3 h from the irradiation. Data represent mean of fluorescence intensity ± SEM of four independent experiments. $^{**}p < 0.01$ versus UVA-irradiated cells.

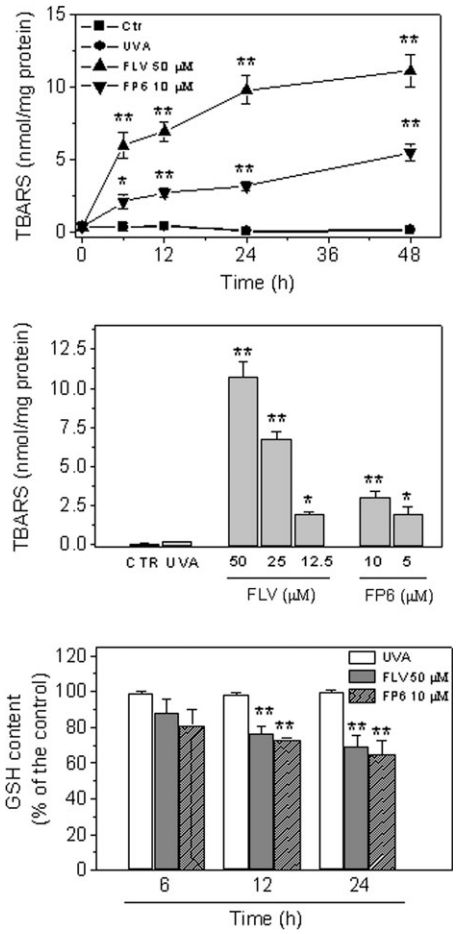

FIG. 12. Panel A) TBARS assay in NCTC-2544 cells after different times from the irradiation (3.75 J/cm^2) with FLV and FP6. Data are expressed as mean ± SEM of three independent experiments. $^{*}p < 0.05$; $^{**}p < 0.01$ versus UVA-irradiated cells. (Panel B) TBARS assay in NCTC-2544 cells after 24 h from the irradiation in the presence of different concentration of FLV and FP6. $^{*}p < 0.05$; $^{**}p < 0.01$ versus UVA-irradiated cells. (Panel C) Relative depletion of GSH content after irradiation in the presence of FLV or FP6. Data are expressed as mean ± SEM of three independent experiments. $^{*}p < 0.05$; $^{**}p < 0.01$ versus UVA-irradiated cells.

analyzed the cellular disposition of FLV and FP6 by fluorescence confocal microscopy, and the results did not show a distinct subcellular localization pattern but only a diffuse signal distributed in the cytoplasm. Further experiments revealed that mitochondria are not affected by the irradiation with FLV or FP6, but, on the contrary, lysosomes are damaged as demonstrated by the reduction of LysoTracker Red fluorescence in comparison to nonirradiated cells. Because the acidic internal milieu of lysosomes is partly maintained by the action of an ATP driven proton pump, the lysosomal destabilization induced by FLV could be caused by damage to the ATP-dependent proton pump or the decrease of ATP levels.

In this context, Ollinger and Brunk (1995) have reported that oxidative stress induced by naphthazarin in human hepatocytes is preceded by lysosomal destabilization followed by lipid peroxidation and energy depletion. Moreover, it is interesting to note that in NCTC-2544 cell line, addition of a cathepsin inhibitor prevents the cell death induced by UVA in cells treated with lovastatin, suggesting that lysosomal damage is involved in the observed phenomenon (Quiec *et al.*, 1995).

The cell death induced by FLV and FP6 is accompanied by a reduction of ATP content but not by loss of mitochondrial membrane potential. Although the disruption of mitochondrial membrane potential plays an important role in necrotic and apoptotic processes, a lack of loss of mitochondrial membrane potential has been reported in nonapoptotic cell death (Kim *et al.*, 2005). Given the rapid increase in cell membrane permeability after FLV or FP6 irradiation as evidenced by intracellular Ca^{2+} increase and PI permeability, it is more plausible that these compounds cause considerable damage to the cell membrane structure thereby promoting substantial ATP leakage into the extracellular spaces. As ATP depletion is

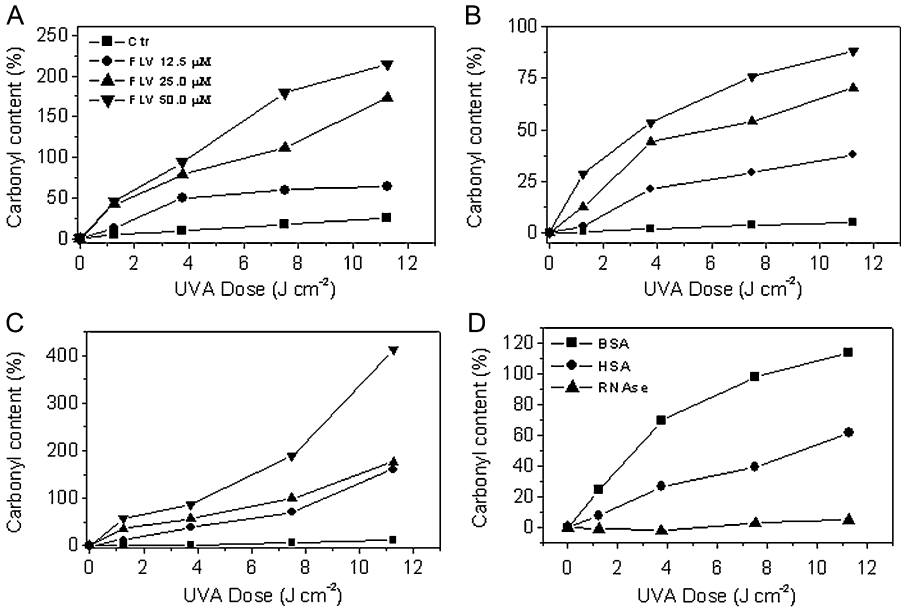

FIG. 13. Photosensitized protein oxidation by FLV and FP6. BSA (panel A), HSA (panel B), and RNAse (panel C), dissolved in phosphate buffer 10mM, pH 7.2, were irradiated at different UVA doses in the presence of FLV at the indicated concentrations and FP6 at the concentration of 10μM (panel D). Protein oxidation was evaluated spectrophotometrically, by monitoring the carbonyl content after derivatization with 2,4-dinitrophenylhydrazine.

thought to be the major cause of necrotic cells death, such loss of the ATP pool may lead to necrosis. However, we cannot exclude the possibility that the drugs may inhibit oxidative phosphorylation without any changes in mitochondrial membrane potential or that the reduction in ATP concentration could be because of an increase in ATP consumption.

The assessment of GSH content and TBARS formation revealed a marked oxidative stress in cells irradiated in the presence of FLV and FP6. GSH is the main non-protein antioxidant in the cell and is able to clear away the superoxide anion and provides electrons for enzymes such as glutathione peroxidase, which reduces H_2O_2 to H_2O. Our results demonstrated that irradiation with FLV or FP6 depleted the intracellular GSH content in keratinocytes supporting the idea that intracellular GSH levels are related to the photoinduced cell death (Higuchi, and Yoshimoto, 2002). To sustain this hypothesis, we have observed an efficient protection from the cell death in the presence of exogenously GSH. Moreover, it also could possible that end products of lipid peroxidation such as 4-hydroxy-2-nonenal can react with the sulfhydryl group of GSH and subsequently cause the reduction of GSH levels (Kinter and Roberts, 1996).

In summary, we have established for the first time that FLV is endowed with a clear phototoxic potential *in vitro* in a human keratinocyte cell line and also in 3T3 fibroblasts. Its phototoxicity could be mediated by the formation of a photoproduct endowed with high photosensitizing properties. We also identified plasma membrane as one of the major targets of the FLV action, which ultimately leads to necrosis as the principal mode of cell death. The photoproduct formation and the possible consequences on the biological effects of the photosensitization of cutaneous cells in patients treated with FLV deserve further studies.

SUPPLEMENTARY DATA

Supplementary data are available online at http://toxsci.oxfordjournals.org/.

FUNDING

Polish State Committee on Science (project no. N N405 3478 33 to K.B.N.).

REFERENCES

Alexander, K. P., Blazing, M. A., Rosenson, R. S., Hazard, E., Aronow, W. S., Smith, S. C., Jr., and Ohman, E. M. (2009). Management of hyperlipidemia in older adults. *J Cardiovasc. Pharmacol. Ther.* **14,** 49–58.

Antunes, F., Cadenas, E., and Brunk, U. T. (2001). Apoptosis induced by exposure to a low steady state concentration of H_2O_2 is a consequence of lysosomal rupture. *Biochem J.* **356,** 549–555.

Astarita, M., Della Greca, M., Iesce, M. R., Montanaro, S., Previtera, L., and Temussi, F. (2007). Polycyclic compounds by sunlight exposure of the drug rosuvastatin in water. *J. Photochem. Photobiol. A* **187,** 263–268.

Beijersbergen van Henegouwen, G. M. J. Medicinal photochemistry (phototoxic and phototherapeutic aspect of drugs). In *Advances in Drug Research.* (B. Testa, and U. Mayer, Eds.), Vol. 29, pp. 79–170. Academic Press, New York.

Cermola, F., Della Greca, M., Iesce, M. R., Montanaro, S., Previtera, L., Temussi, F., and Brigante, M. (2007). Irradiation of fluvastatin in water

structure elucidation of photoproducts. *J. Photochem. Photobiol. A Chem.* **189,** 264–271.

Cermola, F., Della Greca, M., Iesce, M. R., Montanaro, S., Previtera, L., and Temussi, F. (2006). Photochemical behavior of the drug atorvastatin in water. *Tetrahedron* **62,** 7390–7395.

Cosa, G. (2004). Photodegradation and photosensitization in pharmaceutical products: assessing drug phototoxicity. *Pure Appl. Chem.* **76,** 263–275.

Eguchi, Y., Shimizu, S., and Tsuijmoto, Y. (1997). Intracellular ATP levels determine the cell death fate by apoptosis or necrosis. *Cancer Res.* **57,** 1835–1840.

Elisei, F., Aloisi, G. G., Barbafina, A., Dall'Acqua, F., Mazzuccato, U., Canton, M., Facciolo, L., Latterini, L., and Viola, G. (2004). Photophysical and photobiological behaviour of antimalarial drugs in aqueous solutions. *Photochem. Photobiol.* **79,** 248–258.

Ferguson, J. (2002). Photosensitivity due to drugs. *Photodermatol. Photoimmunol. Photomed* **18,** 262–269.

Galluzzi, L., Aaronson, S. A., Abrams, J., Alnemri, E. S., Andrews, D. W., Baehrecke, E. H., Bazan, N. G., Blagosklonny, M. V., Blomgren, K., Borner, C., *et al*. (2009). Guidelines for the use and interpretation of assays for monitoring cell death in higher eukaryotes. *Cell Death Differ.* **16,** 1093–1107.

Girotti, A. W. (2001). Photosensitized oxidation of membrane lipids: reaction pathways, cytotoxic effects, and cytoprotective mechanisms. *J Photochem. Photobiol. B* **63,** 103–113.

Golstein, P., and Kroemer, G. (2007). Cell death by necrosis: toward a molecular definition. *Trends Biochem. Sci.* **32,** 37–43.

Grobelny, P., Viola, G., Vedaldi, D., Dall'Acqua, F., Gliszczynska-Swiglo, A., and Mielcarek, J. (2009). Photostability of pitavastatin: a novel HMG-CoA reductase inhibitor. *J. Pharm. Biomed. Anal.* **50,** 597–601.

Hedley, D. W., and Chow, S. (1994). Evaluation of methods for measuring cellular glutathione content using flow cytometry. *Cytometry* **15,** 349–358.

Higuchi, Y. (2004). Glutathione depletion-induced chromosomal DNA fragmentation associated with apoptosis and necrosis. *J. Cell. Mol. Med* **8,** 455–464.

Higuchi, Y., and Yoshimoto, T. (2002). Arachidonic acid converts the glutathione depletion-induce apoptosis to necrosis by promoting lipid peroxidation and reducing caspase-3 activity in rat glioma cells. *Arch. Biochem. Biophys.* **400,** 133–140.

Holme, S. A., Pearse, A. D., and Anstey, A. V. (2002). Chronic actinic dermatitis secondary to simvastatin. *Photodermatol. Photoimmunol. Photomed* **18,** 313–314.

Kessel, D., and Luo, Y. (2001). Intracellular sites of photodamage as a factor in apoptotic cell death. *J. Porphyrins Phthalocyanines* **5,** 181–184.

Kim, W. H., Choi, C. H., Kang, S., Kwon, C. H., and Kim, Y. K. (2005). Ceramide induces non-apoptotic cell death in human glioma cells. *Neurochem. Res.* **30,** 969–979.

Kinter, M., and Roberts, J. R. (1996). Glutathione consumption and glutathione peroxidase inactivation in fibroblast cell lines by 4-hydroxy-2-nonenal. *Free Radic. Biol. Med.* **21,** 457–462.

Kumar, S. (2007). Caspase function in programmed cell death. *Cell Death Differ* **14,** 32–43.

Leist, M., Single, B., Castoldi, A. F., Kuhnle, S., and Nicotera, P. (1997). Intracellular adenosine triphosphate (ATP) concentration: a switch in the decision between apoptosis and necrosis. *J. Exp. Med.* **185,** 1481–1486.

Levine, L. R. D., Garland, C. N., Oliver, A., Amici, I., Climent, A. G., Lenz, B. G., Ahn, S., Shaltiel, G., and Stadtman, E. R. (1990). Determination of carbonyl content in oxidatively modified proteins. *Methods Enzymol* **186,** 464–480.

Mielcarek, J., Kula, M., Zych, R., and Grobelny, P. (2005). Kinetic studies on fluvastatin photodegradation in solutions. *React. Kinet. Catal. Lett.* **86,** 119–126.

Montanaro, S., Lhiaubet-Vallet, V., Iesce, M. R., Previtera, L., and Miranda, M. A. (2009). A mechanistic study on the phototoxicity of atorvastatin: singlet oxygen generation by a phenanthrene-like photoproduct. *Chem. Res. Toxicol.* **22,** 173–178.

Morliére, P., Mysan, A., Santus, R., Huppe, R., Mazière, J. C., and Dubertret, L. (1991). UVA-induced lipid peroxidation in cultured human fibroblast. *Biochim. Biophys. Acta* **1084,** 261–268.

Nohl, H., Gille, L., and Staniek, K. (2005). Intracellular generation of reactive oxygen species by mitochondria. *Biochem. Pharmacol.* **69,** 719–723.

Oleinick, N. L., Morris, R. L., and Belichenko, I. (2002). The role of apoptosis in response to photodynamic therapy: What, where, why and how. *Photochem. Photobiol. Sci.* **1,** 1–21.

Ollinger, K., and Brunk, U. T. (1995). Cellular injury induced by oxidative stress is mediated through lysosomal damage. *Free Radic. Biol. Med.* **19,** 565–574.

Ouedraogo, G., Morliere, P., Bazin, M., Santus, R., Kratzer, B., Miranda, M. A., and Castell, J. V. (1999). Lysosomes are sites of fluoroquinolone photosensitization in human skin fibroblasts: a microspectrofluorometric approach. *Photochem. Photobiol.* **70,** 123–129.

Porter, A. G., and Janicke, R. U. (1999). Emerging role of caspase-3 in apoptosis. *Cell Death Differ.* **6,** 99–104.

Quiec, D., Mazière, C., Auclair, M., Santus, R., Gardette, J., Redziniak, G., Franchi, J., Dubertret, L., and Mazière, J. C. (1995). Lovastatin enhances the photocytotoxicity of UVA radiation towards cultured N.C.T.C. 2544 human keratinocytes: prevention by cholesterol supplementation and by a cathepsin inhibitor. *Biochem. J* **310,** 305–309.

Rothe, G., and Valet, G. (1990). Flow cytometric analysis of respiratory burst activity in phagocytes with hydroethidine and 2′,7′-dichlorofluorescein. *J. Leukoc. Biol.* **47,** 440–448.

Salvioli, S., Ardizzoni, A., Franceschi, C., and Cossarizza, A. (1997). JC-1 but not DiOC6(3) or rhodamine 123 is a reliable fluorescent probe to asses changes in intact cells: Implications for studies on mitochondrial functionality during apoptosis. *FEBS Lett.* **411,** 77–82.

Shaw, S. M., Fildes, J. E., Yonan, N., and Williams, S. G. (2009). Pleiotropic effects and cholesterol-lowering therapy. *Cardiology* **112,** 4–12.

Spielmann, H., Balls, M., Dupuis, J., Pape, W. J. W., Pechvith, G., and De Silva, O. (1998). The international EU/COLIPA in vitro phototoxicity validation study: results of the Phase II (blind trial); part 1: The 3T3 NRU phototoxicity test. *Toxicol. In Vitro* **12,** 305–327.

Stadtman, E. R., and Levine, R. L. (2003). Free radical-mediated oxidation of free amino acids and amino acid residues in proteins. *Amino Acids* **25,** 207–218.

Stahlmann, R., and Lode, H. (1999). Toxicity of quinolones. *Drugs* **9**(Suppl. 2), 37–42.

Vermes, I., Haanen, C., Steffens-Nakken, H., and Reutelingsperger, C. P. (1995). A novel assay for apoptosis. Flow cytometric detection of phosphatidylserine expression on early apoptotic cells using fluorescein labelled Annexin V. *J. Immunol. Method* **184,** 39–51.

Viola, G., and Dall'Acqua, F. (2006). Photosensitization of biomolecules by phenothiazine derivatives. *Curr. Drug Targets* **7,** 1135–1154.

Viola, G., Salvador, A., Cecconet, L., Basso, G., Dall'Acqua, F., Vedaldi, D., Aloisi, G., Elisei, F., Latterini, L., and Barbafina, A. (2007). Photophysical properties and photobiological behaviour of amodiaquine, chloroquine and primaquine. *Photochem. Photobiol.* **83,** 1415–1427.

Yuan, M. X., Li, W., Dalen, H., Lotem, J., Kama, R., Sachs, L., and Brunk, U. T. (2002). Lysosomal destabilization in p53 induced apoptosis. *Proc. Natl. Acad. Sci. U.S.A.* **99,** 6286–6291.